A Nyström scheme with rational quadrature applied to edge crack problems

Englund, Jonas

Published in:
Communications in Numerical Methods in Engineering

DOI:
10.1002/cnm.93

2007

A Nyström scheme with rational quadrature applied to edge crack problems

J. Englund*,†

Numerical Analysis, Centre for Mathematical Sciences, Lund University, Box 118, SE-221 00, Lund, Sweden

SUMMARY

The effects of introducing rational quadrature into a recently developed algorithm for the computation of the stress field in edge-cracked specimens are studied. The algorithm is based on an integral equation of the second kind which is solved using a Nyström method. Rational quadrature can handle the presence of corners and triple-junctions in a more accurate manner than polynomial quadrature. A preconditioner is also included in the scheme. The rational quadrature together with the preconditioner results in a scheme that reduces the number of discretization points needed for a certain accuracy by up to 70% and the number of iterations needed by an iterative solver by up to 50%, compared to a scheme using only polynomial quadrature. For validation, several setups with a single edge crack are studied. Two large setups, containing 300 and 1500 edge cracks, respectively, are also investigated.

KEY WORDS: stress intensity factor; integral equation; quadrature; preconditioner; fast multipole method; edge crack

1. INTRODUCTION

Using boundary integral equation methods for the solution of certain types of problems can be very beneficial. A commonly mentioned advantage of such methods is the dimensional reduction appearing for instance when the stress field in an isotropic linearly elastic material is computed. One way to discretize and solve an integral equation is by using a Nyström method. For some problems it is fairly easy to construct high-order Nyström schemes, while for other problems care must be taken to retain the high order. For instance, if boundaries containing corners and triple-junctions are studied, kernels appearing in an integral equation formulation will typically behave as rational functions close to the corners. Use of polynomial Gaussian quadrature instead of quadrature more adapted to the situation at hand will negatively

†E-mail: jonase@maths.lth.se
*Correspondence to: J. Englund, Numerical Analysis, Centre for Mathematical Sciences, Lund University, Box 118, SE-221 00, Lund, Sweden

Contract/grant sponsor: The Swedish Research Council; contract/grant number: 621-2001-2799

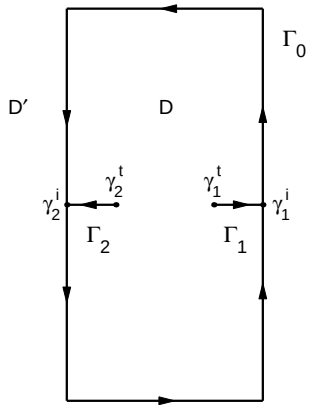

Figure 1. Example of a geometry with two edge cracks. The figure shows the positive orientation of Γ and the notation used throughout this paper.

influence the accuracy of the numerical solution. The main goal of the present paper is to construct a scheme that treats corners and triple-junctions in a more accurate way using rational quadrature. The problems considered below consist of computing stress fields in isotropic linearly elastic domains containing a number of edge cracks.

Section 2 introduces the second kind integral equation that is solved in all numerical experiments in the paper. The same equation was solved in [1] without the special treatment of corners and triple-junctions introduced here. Section 3 describes how efficient quadrature rules can be constructed for parts of the boundary that are close to corners and triple-junctions. Section 4 introduces a simple preconditioner which reduces the number of iterations needed by the iterative solver GMRES with up to 50%. Finally, Section 5 contains comparisons between the new scheme and the scheme used in [1]. The comparisons include some setups containing one edge crack and one setup containing 300 edge cracks. It is also demonstrated that the present scheme can handle setups with 1500 edge cracks as accurately as the earlier scheme handled 300 edge cracks, using similar numbers of discretization points.

2. PROBLEM STATEMENT AND A SECOND KIND INTEGRAL EQUATION

The problem at hand consists of computing the stress field in a finite and simply-connected isotropic linearly elastic specimen when prescribed traction is applied to its boundary. The problems considered are two-dimensional and they all resemble the geometry shown in Fig. 1. We also assume that no body forces are present and that the prescribed traction is such that the specimen is in equilibrium. The domain in $\mathbb{R}^2$ (or in $\mathbb{C}$) that contains the specimen is denoted by D, and its exterior by D'. The boundary of D consists of the outer boundary, denoted by Γ_0, and N_c edge cracks, denoted by Γ_m, $m = 1, \ldots, N_c$. We also need the notation $\Gamma_c = \bigcup_{m=1}^{N_c} \Gamma_m$, and $\Gamma = \Gamma_0 \cup \Gamma_c$. The outer boundary Γ_0 is given positive orientation, and the edge cracks are oriented from crack tip towards Γ_0, see Fig. 1. In all setups considered below the outer boundary, Γ_0, contains four corners.

It is well known that Airy's stress function, $W(x, y)$, $(x, y) \in D \cup D'$, can be represented as

$$W(x,y) = \Re e\{\bar{z}\varphi(z) + \chi(z)\}, \tag{1}$$

where $\varphi(z)$ and $\chi(z)$ are analytic functions of the complex variable $z = x + \mathrm{i}y$. Introduce $\Phi(z) = \varphi'(z)$ and $\Psi(z) = \chi''(z)$ and the Cauchy potentials

$$\Phi(z) = \frac{1}{2\pi\mathrm{i}} \int_\Gamma \frac{\Omega(\tau)\,\mathrm{d}\tau}{\tau - z}, \quad z \in D \cup D', \tag{2}$$

$$\begin{aligned} \Psi(z) &= -\frac{1}{2\pi\mathrm{i}} \int_\Gamma \frac{\overline{\Omega(\tau)}\,\mathrm{d}\bar{\tau}}{\tau - z} - \frac{1}{2\pi\mathrm{i}} \int_\Gamma \frac{\bar{\tau}\Omega(\tau)\,\mathrm{d}\tau}{(\tau - z)^2} \\ &- \frac{1}{2\pi\mathrm{i}} \int_\Gamma \frac{\overline{n(\tau) t^{\mathrm{pr}}(\tau)}\,\mathrm{d}\tau}{\tau - z}, \quad z \in D \cup D', \end{aligned} \tag{3}$$

where $\Omega(z)$ is an unknown layer density on Γ, where $n = n(z)$ is the unit normal to Γ and where $t^{\mathrm{pr}}(z)$ denotes prescribed traction. Once $\Phi(z)$ and $\Psi(z)$ have been determined, the stress state in $D \cup D'$ is known via the Kolosov formulae

$$\sigma_{xx} + \sigma_{yy} = 4\Re e\{\Phi(z)\}, \quad z \in D \cup D', \tag{4}$$

$$\sigma_{yy} - \sigma_{xx} - 2\mathrm{i}\sigma_{xy} = 2(z\overline{\Phi'(z)} + \overline{\Psi(z)}), \quad z \in D \cup D'. \tag{5}$$

Using the potentials (2) and (3) it is possible to derive the following integral equation of the second kind for the problem at hand [1]

$$\left[I - \rho M_1 \rho^{-1} (M_3 + h(\mathrm{i}P_0 + \bar{z}Q))\right] \Omega(z) = \rho M_1 \rho^{-1} g(z), \quad z \in \Gamma. \tag{6}$$

The integral operators in Equation (6) are defined by

$$M_1 f(z) = \frac{1}{\pi\mathrm{i}} \int_\Gamma \frac{f(\tau)\,\mathrm{d}\tau}{\tau - z}, \quad z \in \Gamma, \tag{7}$$

$$\begin{aligned} M_3 f(z) &= \frac{1}{2\pi\mathrm{i}} \int_\Gamma \frac{f(\tau)\,\mathrm{d}\tau}{\tau - z} + \frac{\bar{n}}{n} \frac{1}{2\pi\mathrm{i}} \int_\Gamma \frac{f(\tau)\,\mathrm{d}\tau}{\bar{\tau} - \bar{z}} \\ &+ \frac{1}{2\pi\mathrm{i}} \int_\Gamma \frac{\overline{f(\tau)}\,\mathrm{d}\bar{\tau}}{\bar{\tau} - \bar{z}} + \frac{\bar{n}}{n} \frac{1}{2\pi\mathrm{i}} \int_\Gamma \frac{(\tau - z)\overline{f(\tau)}\,\mathrm{d}\bar{\tau}}{(\bar{\tau} - \bar{z})^2}, \quad z \in \Gamma, \end{aligned} \tag{8}$$

$$Qf = \frac{1}{\pi\mathrm{i}} \int_\Gamma f(z)\,\mathrm{d}z, \tag{9}$$

and

$$P_0 f = -\frac{1}{2A} \Re e \left\{ \int_{\Gamma_0} f(z)\bar{z}\,\mathrm{d}z \right\}, \tag{10}$$

where A denotes the area of D. Let γ_m^{t} denote the crack tip of Γ_m, and let γ_m^{i} denote the point where Γ_m intersects with Γ_0, see Fig. 1. The functions $h(z)$ and $\rho(z)$ appearing in Equation (6) are defined by

$$h(z) = \begin{cases} 1, & z \in \Gamma_0, \\ 0, & z \in \Gamma_c, \end{cases} \tag{11}$$

and

$$\rho(z) = \begin{cases} -\rho_c(z), & z \in D \cup \Gamma_c, \\ \rho_c(z), & z \in D' \cup \Gamma_0, \end{cases} \tag{12}$$

where

$$\rho_c(z) = \prod_{m=1}^{N_c} \left\{ (z - \gamma_m^{\mathrm{i}})^{1/2} \cdot (z - \gamma_m^{\mathrm{t}})^{-1/2} \right\}. \tag{13}$$

The value of $\rho_c(z)$ for $z \in \Gamma$ is defined as the limit from the right relative to the orientation of Γ. Furthermore, we choose the branch given by a branch cut along Γ_c and

$$\lim_{z \to \infty} \rho_c(z) = 1. \tag{14}$$

The right hand side of Equation (6) is given by

$$g(z) = \frac{\bar{n} t^{\mathrm{pr}}(z)}{2} + \frac{\bar{n}}{n} \frac{1}{2\pi \mathrm{i}} \int_\Gamma \frac{n(\tau) t^{\mathrm{pr}}(\tau) \, \mathrm{d}\bar{\tau}}{\bar{\tau} - \bar{z}}, \quad z \in \Gamma. \tag{15}$$

3. RATIONAL QUADRATURE

This section will introduce the main idea of the present paper. In a previous scheme [1], ordinary Gauss-Legendre and Gauss-Jacobi quadrature was used around corners and triple-junctions. This will be avoided here. Instead we will use quadrature rules that are specifically constructed to handle integrals appearing in the operators M_3 and $M_1 \rho^{-1}$, when corners and triple-junctions are present. A similar idea but with a different approach than taken here can be found in [2]. Examples of other methods which are in one way or another related to the problems addressed in the present section can be found in [3, 4, 5, 6], and in the references therein.

One way of solving Equation (6) is by using a Nyström method. This means that the integral operators appearing in the equation are approximated using numerical integration schemes. Typically, one uses composite quadrature rules. That is, Γ is divided into a number of quadrature panels. On each such panel a one-dimensional quadrature rule is used. The solution of Equation (6), $\Omega(z)$, is found at the quadrature nodes. The term discretization points will also be used to denote the quadrature nodes. A discretization point will be referred to as a target point when it plays the role of a point where Equation (6) should be satisfied. A discretization point will be referred to as a source point when it plays the role of quadrature node in the discretization of an integral operator. We will discretize the boundary Γ in such a way that no panel extends over a corner or across a triple-junction. That is, the panels closest to a corner or a triple-junction has one end-point at the corner/triple-junction, see Fig. 2. These panels will be referred to as corner and triple-junction panels.

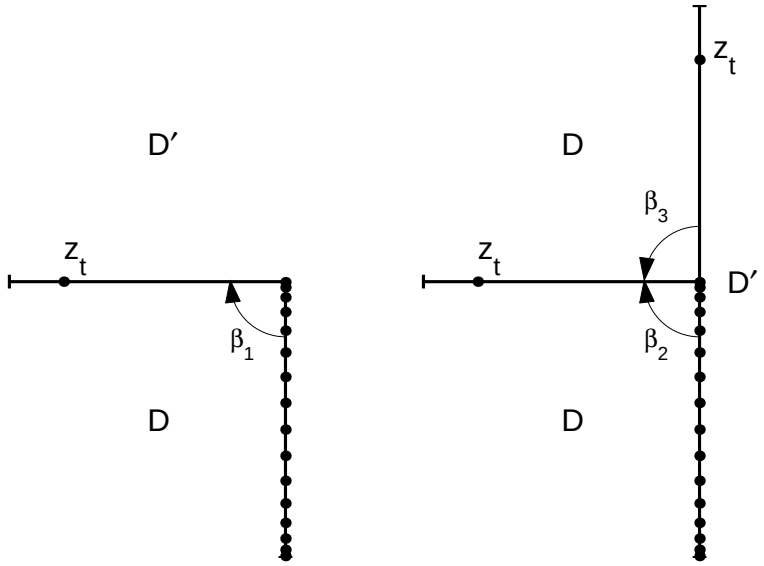

Figure 2. Panel placement around corners (left) and triple-junctions (right). The quadrature nodes for one panel are shown. Points denoted by z_t are examples of target points where rational quadrature is needed for source points on the panel with shown quadrature nodes.

A straightforward choice of numerical quadrature within the Nyström method is to use Gauss-Legendre or Gauss-Jacobi rules on each panel. For boundaries devoid of corners and triple-junctions, polynomial Gaussian quadrature is a good choice. The operator M_3 is then compact when operating on square integrable functions. Furthermore, standard methods, see for instance Section 5 of [7], to compute $M_1\rho^{-1}f(z)$ in the Cauchy principal value sense give accurate results. When Γ contains corners or triple-junctions the kernels appearing in Equation (6) will behave as rational functions when target points and source points are close to and on opposite sides of a corner or a triple-junction, see Fig. 2. Hence, polynomial Gaussian quadrature will no longer be a good choice for such a situation. Instead we will construct simple 16-point interpolatory quadrature rules for corner and triple-junction panels. The reason for using a quadrature rule of order 16 is that it was found to be the best trade-off between accuracy and stability.

We now turn to the construction of the desired quadrature rules. Let Γ_p be a corner or triple-junction panel which is parametrized using a real variable t. That is, $\Gamma_p = \{z(t) : t_s \leq t \leq t_e\}$. We assume that $z(t_s)$ is either a corner or a triple-junction. Let t_j, $j = 0, \ldots, 15$ be the quadrature nodes of 16-point Gauss-Jacobi quadrature, with exponent $-1/2$ at $t = -1$ and exponent 0 at $t = 1$, scaled to the interval $[t_s, t_e]$. One should note that other choices of node placements could also be made with good results. The choice of node placement is not so important. The discretization points on Γ_p are given by $z(t_j)$, $j = 0, \ldots, 15$. Now, define the linear mapping $B(z) = Cz + \alpha$, where C and α are complex constants. We require that $B(z(t_s)) = -1$ and $B(z(t_e)) = 1$, see Fig. 3. Let $z_t \in \mathbb{C} \setminus \Gamma_p$, and let a_j, $j = 0, \ldots, 15$, be complex constants. The quadrature rules we are interested in are such that functions of the

type

$$q_{\mathrm{r}}(\tau) = \sum_{j=0}^{13} a_j \tau^j + \frac{a_{14}}{\tau - B(z_t)} + \frac{a_{15}}{(\tau - B(z_t))^2}, \quad \tau \in B(\Gamma_p), \tag{16}$$

are integrated exactly over $B(\Gamma_p)$. Note that the quadrature weights in general will be complex. This particular choice of $q_{\mathrm{r}}(\tau)$ is motivated by the structure of the operators M_1 and M_3 as defined by (7) and (8), respectively. Let $P_n(\tau)$ be a complex valued polynomial of degree n. The definition of $q_{\mathrm{r}}(\tau)$ implies that rational functions of the types $P_{14}(\tau)/(\tau - B(z_t))$ and $P_{15}(\tau)/(\tau - B(z_t))^2$ are integrated exactly, and these functions are appropriate approximations of the integrands that appear in M_1 and M_3. Quadrature weights for the last three integrals in the definition (8) of M_3, which contain denominators that are conjugated compared to the definition of $q_{\mathrm{r}}(\tau)$, are given by the conjugates of quadrature weights obtained for $q_{\mathrm{r}}(\tau)$. For the operator $M_1\rho^{-1}$ and quadrature panels closest to a triple-junction one modification must be done in order to ensure that the square-root singularities of $\rho(z)^{-1}$ at the triple-junctions are captured by the quadrature. We therefore demand that $(\tau+1)^{-1/2}q_{\mathrm{r}}(\tau)$ rather than $q_{\mathrm{r}}(\tau)$ should be integrated exactly for this situation.

The above choice of $q_{\mathrm{r}}(\tau)$ has the consequence that the leading term of a series expansion of $\Omega(z)$ around a corner or triple-junction is integrated exactly for certain geometries. When $\beta_1 < \pi$ or when $\max(\beta_2, \beta_3) < \pi$, see Fig. 2, the leading term of a series expansion of $\Omega(z)$ will be a constant [8] and such a term is present in $q_{\mathrm{r}}(\tau)$ of (16). The exponents of the higher order terms of the series expansion will in general be complex numbers with irrational real and imaginary parts. Therefore only the leading term of the expansion is integrated exactly using the quadrature described here. This is however, as will be shown in the numerical experiments below, enough to achieve a significant improvement when compared to the scheme in [1], where polynomial quadrature is used. Note that if geometries with any angle β_i larger than π are to be investigated, the scheme presented here will need some modifications in order to be effective. At corners and triple-junctions with such angles, the solution $\Omega(z)$ will be singular, which is not accounted for in the definition of $q_{\mathrm{r}}(\tau)$.

For the discretization of integrals over a corner or triple-junction panel we will need one set of quadrature weights for each target point that is close enough to the panel under consideration. When the distance of a target point from a corner/triple-junction panel is approximately longer than the length of the corner/triple-junction panel, no rational quadrature is needed since polynomial and rational quadrature then give equally accurate results. We therefore only construct rational quadrature rules for the following situations:

- Source points on one corner panel and target points on the other corner panel at that corner.
- Source points on a triple-junction panel and target points on the other two triple-junction panels at that triple-junction.

Source points on corner/triple-junction panels and target points not included in the two above situations are treated using a set of quadrature weights which comes from the requirement that functions of the type

$$q_{\mathrm{p}}(\tau) = \sum_{j=0}^{15} a_j \tau^j, \quad \tau \in [-1, 1], \tag{17}$$

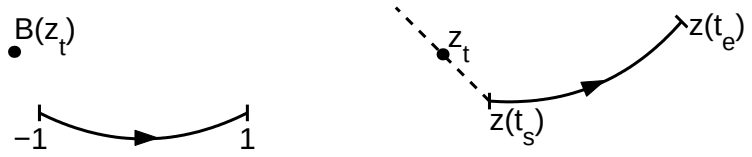

Figure 3. Left, the position of $B(\Gamma_p)$ and $B(z_t)$. Right, the position of Γ_p and z_t. Note that a corner or triple-junction is present at $z(t_s)$.

should be integrated exactly over $[-1, 1]$. Since this set of weights is independent of z_t, the same set can be used for all corner and triple-junction panels. Note that if the nodes on corner/triple-junction panels are placed according to Gauss-Legendre quadrature, the weights resulting from the requirement of exact integration of q_{p}, will be the usual Gauss-Legendre weights.

The above means that, for each corner, 32 sets of 16 quadrature weights are computed. For each triple-junction, 192 sets of 16 quadrature weights are computed (since M_3 and $M_1\rho^{-1}$ need separate weights, we have to compute 192 rather than 96 sets of weights at triple-junctions).

The requirement that a quadrature rule integrates either $q_{\mathrm{r}}(\tau)$ or $(\tau+1)^{-1/2}q_{\mathrm{r}}(\tau)$ exactly leads to ill-conditioned 16×16 linear systems for the weights. The condition numbers for the target points that are located closest to a corner or triple-junction typically are on the order of 10^6. For target points farther away the condition numbers are larger. When the distance from a target point to a corner/triple-junction panel is approximately equal to the length of the corner/triple-junction panel, the condition number can be as large as 10^{12}. Therefore the systems are solved using Gaussian elimination performed in quadruple precision. Once the quadrature weights have been computed they are truncated to double precision prior to running the main part of the algorithm.

Advantages of the quadrature rules described here compared to more elaborate methods as can be found in, for instance, [8] are:

- It can easily and automatically handle setups containing many different angles β_i, $i = 1, 2, 3$, see Fig. 2.
- It can handle non-straight corner and triple-junction panels.
- There is no need for a time consuming pre-processor using adaptive quadrature since integrals of $q_{\mathrm{r}}(\tau)$ and $(\tau+1)^{-1/2}q_{\mathrm{r}}(\tau)$ can be computed analytically.

4. A SIMPLE PRECONDITIONER

This section introduces a preconditioner that is based on a splitting of integral operators, appearing in Equation (6), into two parts. One part contains close range interactions for the

situation when both target and source points are close to a corner or triple-junction. The other part contains close range interactions for the situation when target and source points are not close to a corner or triple-junction. The second part also contains long range interactions. If polynomial quadrature is used around corners and triple-junctions the computational mesh must be refined there if highly accurate solutions are desired. In the refined mesh a large number of discretization points will be placed close to the corners and triple-junctions. Since the cost of our preconditioner depends on the number of such discretization points, an efficient preconditioner will be too expensive. When rational quadrature is used, the need for a refined mesh around corners and triple-junctions is reduced and one can then construct an efficient and cheap preconditioner.

Let Γ_j^p be the union of the two (or three) quadrature panels closest to corner (or triple-junction) j, where the triple-junctions are numbered from 1 to N_c and the four corners from N_c+1 to N_c+4. Define the operator

$$M_1^p f(z) = \begin{cases} \frac{1}{\pi \mathrm{i}} \int_{\Gamma_j^p} \frac{f(\tau)\,\mathrm{d}\tau}{\tau - z}, & z \in \Gamma_j^p, \quad j = 1, \ldots, N_c + 4, \\ 0, & z \in \Gamma \setminus \bigcup_{j=1}^{N_c+4} \Gamma_j^p. \end{cases} \tag{18}$$

The operator M_3^p is defined analogously. One possible way to construct a preconditioner is to rewrite Equation (6) as

$$\left[I - T_b + T_b - \rho M_1 \rho^{-1} (M_3 + h(\mathrm{i}P_0 + \bar{z}Q)) \right] \Omega(z) = \rho M_1 \rho^{-1} g(z), \quad z \in \Gamma, \tag{19}$$

where $T_b = \rho M_1^p \rho^{-1} M_3^p$. The intuitive idea behind this choice of T_b is similar to the one described in Section 8.1 of [9]. Define the operator $T = \rho M_1 \rho^{-1} (M_3 + h(\mathrm{i}P_0 + \bar{z}Q)$, operating on functions in some appropriately weighted L^2-space. What one ideally wants is to split the integral operator T, appearing on the left hand side of Equation (6), into a compact part, T_c, and a non-compact part, T_b. That is, $I - T = I - T_b - T_c$. If $I - T_b$ is left invertible, application of $(I - T_b)^{-1}$ from the left in the original integral equation gives a Fredholm integral equation of the second kind. With our choice of T_b, $T - T_b$ will not be compact. If M_1^p is redefined so that the domain where $M_1^p f(z)$ is non-zero is increased to include both all the Γ_j^p and one or more panels neighboring the Γ_j^p, then $T - T_b$ will be compact. The results of the numerical experiments below were unaltered when M_1^p was modified in such a way. Therefore we opted to use the above definition of M_1^p, which leads to a simpler and faster algorithm. The question of whether the operator $I - T_b$ is left invertible is to the best of our knowledge non-trivial to prove rigorously, but numerical experiments indicate that this indeed is the case. Assume that $I - T_b$ is left invertible and apply $(I - T_b)^{-1}$ from the left in Equation (19). This gives the preconditioned equation

$$\left[I - (I - T_b)^{-1} (\rho M_1 \rho^{-1} (M_3 + h(\mathrm{i}P_0 + \bar{z}Q)) - T_b) \right] \Omega(z) = (I - T_b)^{-1} \rho M_1 \rho^{-1} g(z), \quad z \in \Gamma. \tag{20}$$

Equation (20) is solved numerically in the following section. Informally speaking, Equation (20), is closer to being a Fredholm integral equation of the second kind than Equation (6).

The discretized version of T_b is a block-diagonal matrix and the action of $(I - T_b)^{-1}$ can be computed in a fast manner using LU-factorization since the size of each block will at the most be 96×96.

5. NUMERICAL EXAMPLES

This section will present several experiments where Equation (20) is discretized and solved numerically using a Nyström scheme. Integrals appearing in Equation (20) are discretized using composite quadrature. For quadrature panels that end either at a corner or at a triple-junction, 16-point quadrature as discussed in Section 3 is used. For panels containing a crack tip, 8-point Gauss-Jacobi quadrature with exponent $-1/2$ is used. On the remaining panels, 8-point Gauss-Legendre quadrature is used. The computer code was written in Fortran 77 and compiled using the Sun Fortran 77 compiler. All experiments were performed on a SunBlade 100 workstation.

The linear system of equations resulting from the Nyström scheme was solved using the iterative GMRES solver accelerated with the fast multipole method. Unless explicitly stated otherwise, the GMRES iterations in the experiments below were terminated when the relative residual had reached 10^{-12}.

An a priori adaptive approach was used around corners and triple-junctions. See [7] for details of this adaptive approach. In contrast to the scheme in [1], the rational quadrature used here removes the need for many refinements. One level of refinement gives enough accuracy for most applications. To achieve maximum accuracy no more than 5-7 refinements are needed.

In all experiments traction was prescribed as shown in Fig. 4. That is, traction of unit magnitude was applied along the upper and lower edges of Γ_0.

A description of how the operator M_1 is discretized and how $\rho(z)$ is computed can be found in [1]. To be able to compare the performance of the present scheme with earlier ones, stress intensity factors, F_{I} and F_{II}, and T-stresses were computed. Details regarding the computation of these fracture parameters can also be found in [1].

5.1. RECTANGULAR PLATE WITH ONE EDGE CRACK

In the previous paper [1] several specimens with one straight edge crack of the type shown in Fig. 4 were investigated. The notation of Fig. 4 will be used below.

In the present section four different schemes will be used: The scheme from [1], which will be called the *Poly* scheme. The scheme from [1] with preconditioning as described in Section 4 added, which will be called the *PolyPrec* scheme. A scheme with rational quadrature around corners and triple-junctions but without preconditioning, which will be called the *Rat* scheme. A scheme with both rational quadrature and preconditioning as described in Section 4, which will be called the *RatPrec* scheme.

A convergence test was performed for a setup with $h/w = 1$, $a/w = 0.5$, and $\theta = 0$, see Fig. 5. In the left part of Fig. 5 the RatPrec scheme is compared to the Poly scheme. One level of adaptive refinement was used around corners and triple-junctions. Apparently, the RatPrec scheme clearly outperforms Poly. The error from Poly is approximately proportional to the length of the corner and triple-junction panels. That is, under uniform refinement the Poly scheme is of order one. Already for small meshes the RatPrec scheme gives accurate results and it also converges faster under uniform refinement. The right part of Fig. 5 shows the relative error in F_{I} as a function of the number of performed GMRES iterations for a mesh with 9968 discretization points. The RatPrec scheme reaches the desired residual faster than the Poly scheme. The behaviour of RatPrec, as shown in the left part of Fig. 5, resembles the behaviour shown in Fig. 7 of [8]. The RatPrec scheme can be seen as a simplified but more flexible version

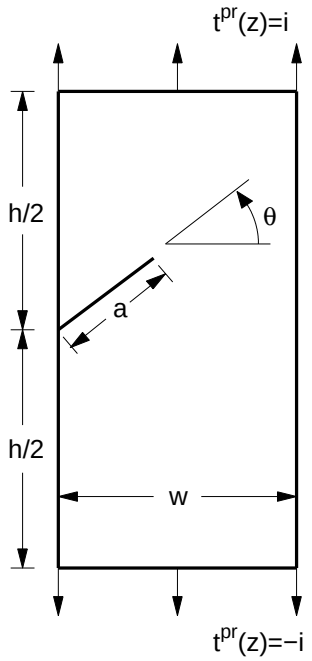

Figure 4. The rectangular plate with one edge crack discussed in Section 5.1.

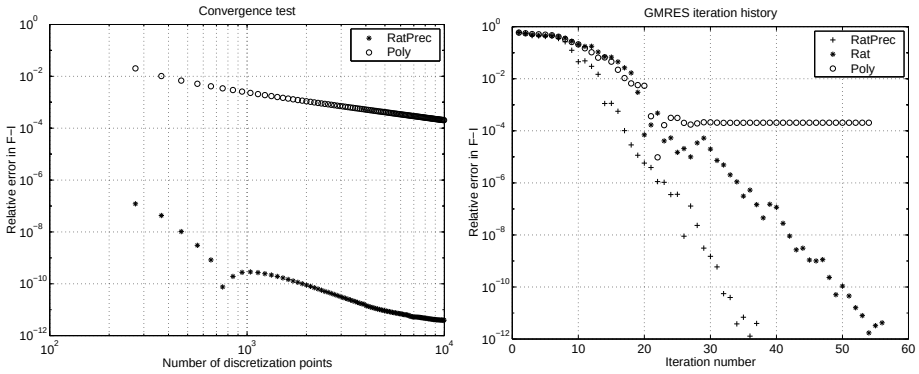

Figure 5. The left figure shows a convergence test comparing the RatPrec scheme with the Poly scheme. See beginning of Section 5.1 for definitions of the Poly and RatPrec schemes. The dimensions of the specimen were $h/w = 1$, $a/w = 0.5$, and $\theta = 0$. The mesh was refined uniformly. As reference we used the value $F_{\mathrm{I}} = 3.0087584653$, which comes from [1]. The right figure shows the development of the relative error in F_{I} for the largest run in the left figure.

of the approach used in [8]. In Fig. 5 it can also be seen that the preconditioner of Section 4 clearly decreases the number of iterations needed.

A couple of tests regarding the impact of the rational quadrature and the preconditioner were made, see Table I. In these tests a mesh that contained no more than 272 discretization points

Table I. Investigation of the impact of the rational quadrature introduced in Section 3 and of the preconditioner introduced in Section 4. In all experiments of this table the number of discretization points was 272. The row denoted Error concerns the relative error in F_{I}. See beginning of Section 5.1 for definitions of the Poly, PolyPrec, Rat, and RatPrec schemes. As reference values we used values presented in Section 7.2 of [1].

h/w	a/w	θ		Poly	PolyPrec	Rat	RatPrec
1	0.5	0	Iterations	48	25	48	25
			Error	$2.0 \cdot 10^{-2}$	$2.0 \cdot 10^{-2}$	$1.2 \cdot 10^{-7}$	$1.2 \cdot 10^{-7}$
2	0.5	0	Iterations	44	25	49	25
			Error	$2.3 \cdot 10^{-3}$	$2.3 \cdot 10^{-3}$	$4.2 \cdot 10^{-7}$	$4.2 \cdot 10^{-7}$
2	0.4	$\pi/6$	Iterations	45	26	50	26
			Error	$1.4 \cdot 10^{-3}$	$1.4 \cdot 10^{-3}$	$8.6 \cdot 10^{-7}$	$8.6 \cdot 10^{-7}$
2	0.5	$\pi/4$	Iterations	49	27	54	27
			Error	$8.7 \cdot 10^{-4}$	$8.7 \cdot 10^{-4}$	$1.5 \cdot 10^{-6}$	$1.5 \cdot 10^{-6}$

was used. The RatPrec scheme decreased the number of iterations needed by about 50% for all setups and also decreased the error significantly, when compared to the Poly scheme.
In [1] the following three tests were made for a couple of rectangular setups: When $\theta = 0$, Test 1 investigates the number of discretization points and iterations needed in order to achieve a relative error smaller than 1% in both F_{I} and T. When $\theta \neq 0$, Test 1 investigates when the relative error was smaller than 1% in both F_{I} and F_{II}. Test 2 investigates the number of discretization points and iterations needed to achieve the same accuracy as in the most accurate results found in the literature. Test 3 investigates the number of discretization points and iterations needed to achieve relative errors in both F_{I} and T (for specimens with $\theta = 0$) or F_{I} and F_{II} (for specimens with $\theta \neq 0$) that are smaller than 10^{-10}. These three tests were performed using the RatPrec scheme and compared to the Poly scheme, see Table II. In these tests the iterations were halted when the relative errors had reached the desired value.
In connection with Table II one should note that the coarsest mesh possible with the present implementation contained 272 discretization points. In [1] the coarsest mesh possible contained 184 discretization points. This is a consequence of the fact that here we have used 16-point quadrature instead of 8-point quadrature around corners and triple-junctions. One should also notice that the errors from the RatPrec scheme using 272 discretization points are typically significantly lower than 1%, which is shown in Table I. From the two rightmost columns in Table II one can see that the RatPrec scheme decreased the number of discretization points needed to achieve relative errors less than 10^{-10} by 65% to 75%.

5.2. RECTANGULAR PLATE WITH MANY EDGE CRACKS

A clear indication of the improvements the ideas in Sections 3 and 4 result in is the maximum number of edge cracks that can be handled. Using the present scheme, we found that we could simulate a specimen containing 1500 cracks as accurately as we could simulate a specimen containing 300 edge cracks using the scheme in [1]. A specimen containing 1500 was constructed by extending the specimen with 300 edge cracks studied in [1], see Fig. 6. Using the notation of Fig. 4 the plate had the dimensions $h = 150$ and $w = 1$. Edge cracks were placed equidistantly

Table II. Results from the three tests mentioned in Section 5.1. The reference values used are presented in Section 7.2 of [1]. The number of discretization points used is denoted by N. Test 1: Relative error less than 10^{-2}. Test 2: Relative error equal to the most accurate result found in the literature. Test 3: Relative error less than 10^{-10}. See beginning of Section 5.1 for definitions of the Poly and RatPrec schemes.

				Test 1		Test 2		Test 3	
h/w	a/w	θ		RatPrec	Poly	RatPrec	Poly	RatPrec	Poly
1	0.5	0	Iterations	11	16	12	16	35	58
			N	272	536	272	712	904	3904
2	0.5	0	Iterations	12	15	13	21	33	51
			N	272	272	272	536	1008	3553
2	0.4	$\pi/6$	Iterations	13	15	14	18	39	58
			N	272	184	272	184	1040	2984
2	0.5	$\pi/4$	Iterations	14	20	18	32	42	70
			N	272	184	272	592	1040	2984

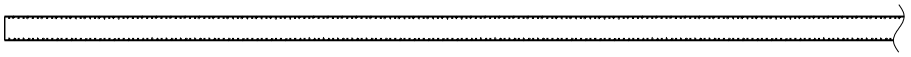

Figure 6. Part of the geometry studied in Section 5.2. Due to the complexity of the geometry only about one fourth of the plate is shown. Note that the specimen has been rotated 90° in this figure. The specimen contains 1500 edge cracks and is loaded by unit traction along the short plate edges.

with 750 cracks along both the right and left edges of the plate. The edge cracks were of the same three types as in the setup with 300 edge cracks: a straight crack with $\theta = 0$ and $a = 0.1$, a straight crack with $\theta = \pi/6$ and $a = 0.1$, and a non-straight crack. See Fig. 4 for a definition of a and θ. The non-straight crack consisted of part of a circle with radius r and opening angle β. Here $r = 1/3$ and $\beta = \pi/10$ which means that this crack type had length $a = \pi/30$. The angle between the non-straight cracks and the plate edges, at the points of intersection, was $\pi/2$. The distance, along the plate edge, between two consecutive cracks was $h/751$. For a more detailed picture of how the specimens in the present section were constructed, see the figures in Section 7.3 of [1].

In [1] the smallest error obtained for the specimen containing 300 edge cracks was approximately 10^{-7}, using a total of 205,000 discretization points, see Fig. 9 of [1]. The present

scheme managed to achieve smaller errors for the same setup using only 53,000 discretization points. The error used here is defined as the relative error in $\|\overline{F}_{\rm I}\|_\infty$, in $\|\overline{F}_{\rm II}\|_\infty$, and in $\|\overline{T}\|_\infty$, where $\overline{F}_{\rm I}$, $\overline{F}_{\rm II}$, and $\overline{T}$ are vectors containing numerically computed stress intensity factors and T-stresses for all crack tips. As a final test we investigated the number of discretization points needed by the present scheme to obtain an error of approximately 10^{-7} for a specimen with 1500 edge cracks. It was found that a mesh containing 264,000 points was enough to achieve the desired accuracy. The value of $F_{\rm I}$ for the straight crack in the lower right corner of the plate was found to be $F_{\rm I} = 1.255450$. This was the largest component of $\overline{F}_{\rm I}$. As reference, values from a run with 589,000 discretization points were used.

In addition to being an efficient modification of the scheme in [1], the quadrature discussed in Section 3 can also be used to construct an efficient post-processor for the computation of the entire stress field in a specimen. The need for adaptive refinement will be drastically reduced for the situation when the point where the stress field is computed lies close to Γ. In order to illustrate that the present algorithm can be used to compute the stress field accurately in complicated setups, the von Mises effective stress $\sigma_{\rm e}$ was computed for the specimen containing 1500 edge cracks. For a plane strain state of stress, $\sigma_{\rm e}$ is given by

$$\sigma_{\rm e} = \left[(1-\nu(1-\nu))(\sigma_{xx}+\sigma_{yy})^2 - 3(\sigma_{xx}\sigma_{yy}-\sigma_{xy}^2)\right]^{1/2}, \tag{21}$$

where ν is Poisson's ratio. In order to compute the stress field Equation (20) was solved using 264,000 discretization points. The solution, $\Omega(z)$, was then used together with the Kolosov formulae (4) and (5) to compute effective stresses, see Fig. 7, where we have used $\nu = 0.3$. Because of the complexity of the setup only a small portion of the specimen is shown in the figure.

6. DISCUSSION

Two modifications of a previous scheme for the computation of the stress field in edge-cracked specimens were presented. Quadrature rules that can handle the complicated kernels appearing in Equation (6) were introduced in Section 3. In Section 4 a simple preconditioner was introduced. A scheme which used the rational quadrature in tandem with the preconditioner clearly outperformed the previous scheme both in terms of accuracy for a given mesh size and in terms of iterations needed.

Compared to more elaborate basis functions approaches, the method presented here is more general in the sense that it can easily treat non-straight corner and triple-junction panels. Furthermore, no time consuming adaptive quadrature is needed to construct the rational quadrature of Section 3.

Finally, it should be noted that all computations in the present paper were performed using the same standard workstation as was used in [1].

REFERENCES

1. Englund J. Efficient algorithm for edge cracked geometries. *International Journal for Numerical Methods in Engineering*, available online 12 December 2005.

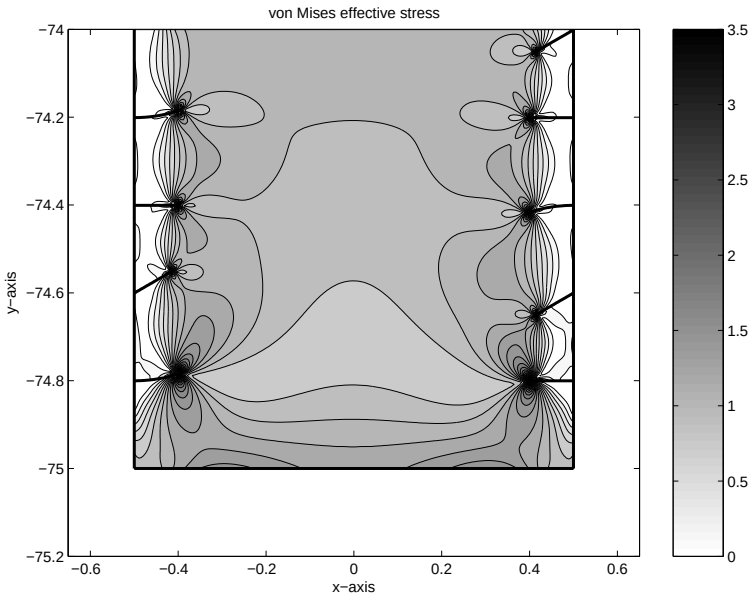

Figure 7. Contour plot of the von Mises effective stress, Equation (21), in a small part of the geometry shown in Fig. 6. Poisson's ratio was set to $\nu = 0.3$. The grid used for the plot contains 40,000 points and shows 25 equidistant lines for effective stresses between 0 and 3.5.

2. Monegato G, Palamara Orsi A. Product formulas for Fredholm integral equations with rational kernel functions. In *Numerical Integration III, International Series in Numerical Mathematics, Vol. 85*, Brass H, Hämmerlin G (eds). Birkhäuser: Basel, 1988; 140-156.
3. Gautschi W. The use of rational functions in numerical quadrature. *Journal of Computational and Applied Mathematics* 2001; **133**(1-2):111-126.
4. Helsing J. Thin bridges in isotropic electrostatics. *Journal of Computational Physics* 1996; **127**(1):142-151.
5. Strain J. Locally corrected multidimensional quadrature rules for singular functions. *SIAM Journal on Scientific Computing* 1995; **16**(4):992-1017.
6. Theocaris PS, Ioakimidis NI. A method of numerical solution of Cauchy-type singular integral equations with generalized kernels and arbitrary complex singularities. *Journal of Computational Physics* 1979; **30**(3):309-323.
7. Englund J. Stable algorithm for the stress field around a multiply branched crack. *International Journal for Numerical Methods in Engineering* 2005; **63**(6):926–946.
8. Helsing J, Jonsson A. On the computation of stress fields on polygonal domains with V-notches. *International Journal for Numerical Methods in Engineering* 2002; **53**(2):433-453.
9. Atkinson KE. *The Numerical Solution of Integral Equations of the Second Kind*. Cambridge University Press: Cambridge, 1997.